Estimating the Noise-Related Error in Continuous-Time Integrator-Based ADCs

Paul Gosselin, Adil Koukab, and Maher Kayal

***Abstract*—From first-order incremental ΣΔ converters to controlled-oscillator-based converters, many ADC architectures are based on the continuous-time integration of the input signal. However, the accuracy of such converters cannot be properly estimated without establishing the impact of noise. In fact, noise is also integrated, resulting in a random error that is added to the measured value. Since drifting phenomena may make simulations and practical measurements unable to ensure long-term reliability of the converters, a theoretical tool is required. This paper presents a solution to compute the standard deviation of the noise-generated error in continuous-time integrator-based ADCs, under the assumption that a previous measure is used to calibrate the system. In addition to produce a realistic case, this assumption allows to handle a theoretical issue that made the problem not properly solvable. The theory is developed, the equations are solved in the cases of pure white noise, pure flicker noise and low-pass filtered white noise, and the implementation issues implied by the provided formulas are addressed.**

***Index Terms*—Noise, White noise, Flicker noise, Error, Accuracy, Standard deviation, Variance, Integrator-based ADC, Incremental, Sigma-Delta.**

I. Introduction

MANY ADC structures are based on integrating the input signal on a given time interval. In fact, when considering converting a signal that is constant or that varies slowly enough, value-to-frequency conversion is often an efficient way to reach high resolution [1], [2].

Such a conversion can be implemented using a current-controlled oscillator as in [3]: the input signal feeds an integrator that is reseted each time its output reaches a given threshold value. Another widely used implementation is the first-order incremental ΣΔ converter, as in [4] and [5]: the integrator output is compared to the threshold value only at the rising edges of the clock, but instead of resetting it, constant values are subtracted to its output.

Besides, when measuring a low current (e.g. the one from a photodiode), integrating it on a capacitance prior to conversion is a practical way to amplify it and translate it into a voltage, which is easier to convert [6].

In any of these cases, what is actually measured is ideally the average value of the input signal $s(t)$ on time interval during which it is integrated $[0,\tau]$: $\langle s\rangle = \frac{1}{\tau}\int_0^\tau s(t)\,\mathrm{d}t$.

However, in practice, a noise signal δs is added to the input signal s. It includes both the noise at the input of the converter and the input referred-noise of the integrator. So, without considering any additional imperfection, what is measured is:

$$s_{meas} = \frac{1}{\tau}\int_0^\tau \left(s(t)+\delta s(t)\right)\,\mathrm{d}t = \langle s\rangle + \varepsilon \qquad (1)$$

Thus the input-referred noise δs results in an error $\varepsilon = \langle \delta s\rangle = \frac{1}{\tau}\int_0^\tau \delta s(t)\,\mathrm{d}t$. This is a random variable having a null expected value and a normal distribution. In order to estimate at best the accuracy of the considered ADC, it is required to estimate the standard deviation σ_ε of this error.

Note that in some contexts and because of drifting phenomena typically due to flicker noise, a theoretical tool is required to estimate this standard deviation. For example, when considering an implanted biomedical sensor that is expected to work for months or even years, simulations and practical measurements may not be sufficient to ensure the reliability of the system.

In the electronics-related literature, trace of this issue can be found back to 1962 [7]. However, only the case of low-pass filtered white noise was considered. More recently, in 2007, [8] addressed the case of pure white noise and pure flicker noise. The obtained standard deviations σ_ε were computed from the formula:

$$\sigma_\varepsilon^2 = \frac{1}{\tau^2}\int_0^\infty \frac{2S(\omega)}{\omega^2}\left[1-\cos(\omega\,\tau)\right]\mathrm{d}\omega \qquad (2)$$

where $S(\omega)$ is the power spectral density of the input-referred noise δs.

However, this integral diverge for $\omega \to 0$ as soon as $S(\omega) \overset{\omega\to 0}{\sim} \frac{A}{\omega^\alpha}$ with $\alpha \geq 1$ (which is typically the case with the noise produced by PMOS). The solution proposed in [8] is to integrate only from a minimal pulsation ω_{min} below which the signal is considered as constant. This solution is not satisfactory. In fact, the arbitrary choice of ω_{min} can considerably impact the computed σ_ε. Actually, if calibration is considered to reject the DC error, the lowest noise frequencies are partially compensated, and the more the frequency increases, the less this compensation occurs. This phenomenon must be taken into account, and doing so will solve the aforementioned convergence issue. Thus, it is proposed to modify the problem to incorporate the effect of calibration.

II. Improving the Theory

We now consider that prior to the actual measure from times 0 to τ, a calibration measure was done using an integration time τ_c ($\tau_c \geq \tau$) and its result is subtracted to the current measure. Let T_c ($T_c \geq \tau_c$) be the elapsed time from the beginning of the calibration to the beginning of the current

P. Gosselin, A. Koukab and M. Kayal are with Electronics Laboratory and Power Systems Laboratory, École Polytechnique Fédérale de Lausanne, Lausanne, Switzerland (e-mail: paul.gosselin@epfl.ch)

measure. Then, the induced random error is:

$$\varepsilon = \langle \delta s \rangle = \frac{1}{\tau}\int_0^{\tau} \delta s(t)\,\mathrm{d}t - \frac{1}{\tau_c}\int_{-T_c}^{-T_c+\tau_c} \delta s(t)\,\mathrm{d}t \quad (3)$$

The demonstration for (2) must then be adapted. δs is first expressed as a Fourier series:

$$\delta s(t) = \sum_{i=1}^{\infty} \sqrt{2\,S(\omega_i)\,\delta\omega}\cos\left(\omega_i t + \delta_i\right) \quad (4)$$

where the δ_i are uncorrelated uniform random variables distributed the interval $[0, 2\pi]$. Then:

$$\varepsilon = \sum_{i=1}^{\infty} \sqrt{2\,S(\omega_i)\,\delta\omega}\;\mathcal{I}(f)$$

with:

$$\mathcal{I}(\omega_i) = \frac{1}{\tau}\int_0^{\tau} \cos\left(\omega_i\,t + \delta_i\right)\mathrm{d}t - \frac{1}{\tau_c}\int_{-T_c}^{-T_c+\tau_c} \cos\left(\omega_i\,t + \delta_i\right)\mathrm{d}t$$

Then, since $\mathrm{E}[\varepsilon] = 0$:

$$\sigma_\varepsilon^2 = \mathrm{E}\left[\varepsilon^2\right] = \mathrm{E}\left[\left(\sum_{i=1}^{\infty}\sqrt{2\,S(\omega_i)\,\delta\omega}\;\mathcal{I}(\omega_i)\right)^2\right]$$

$$= \mathrm{E}\left[\sum_{i=1}^{\infty}\sum_{j=1}^{\infty} 2\,\delta\omega\,\sqrt{S(\omega_i)\,S(\omega_j)}\;\mathcal{I}(\omega_i)\,\mathcal{I}(\omega_j)\right]$$

Since the δ_i are uncorrelated:

$$\forall\; i \neq j,\quad \mathrm{E}[\mathcal{I}(\omega_i)\,\mathcal{I}(\omega_j)] = \mathrm{E}[\mathcal{I}(\omega_i)]\;\mathrm{E}[\mathcal{I}(\omega_j)] = 0$$

So, considering the limit $\delta\omega \longrightarrow 0$:

$$\sigma_\varepsilon^2 = \int_0^{\infty} 2\,S(\omega)\,\mathrm{E}\left[\mathcal{I}(\omega)^2\right]\mathrm{d}\omega$$

$\mathrm{E}\left[\mathcal{I}(\omega)^2\right]$ is then computed as:

$$\mathrm{E}\left[\mathcal{I}(\omega)^2\right] = \frac{1}{2\pi}\int_0^{2\pi} \mathcal{I}(\omega)^2\,\mathrm{d}\delta$$

Ultimately, it leads to:

$$\sigma_\varepsilon^2 = \int_0^{\infty} 2\,S(\omega)\,G\left(\omega\,T_c, \frac{\tau}{T_c}, \frac{\tau_c}{T_c}\right)\mathrm{d}\omega \quad (5)$$

with:

$$G(u,x,y) = \tfrac{1}{u^2}\left[\frac{1}{x^2}\Big(1-\cos(u\,x)\Big) + \frac{1}{y^2}\Big(1-\cos(u\,y)\Big) - \frac{1}{x\,y}\Big(\cos(u) + \cos(u\,(1+x-y)) - \cos(u\,(1+x)) - \cos(u\,(1-y))\Big)\right]$$

From (5), several remarks can be done. First, we note that the aforementioned convergence issue is solved. In fact:

$$G\left(\omega T_c, \frac{\tau}{T_c}, \frac{\tau_c}{T_c}\right) \overset{\omega\to 0}{\sim} \frac{1}{8}\left(4T_c(T_c+\tau-\tau_c) + (\tau-\tau_c)^3\right)\omega^2$$

hence the integral converges as soon as $S(\omega) \overset{\omega\to 0}{=} O\left(\frac{1}{\omega^\alpha}\right)$ with $\alpha < 3$, which is always the case in practice. Besides, the effect of the calibration can be observed. The way the power spectral density is weighted and affects the resulting standard deviation is depicted in Fig. 1. Be the calibration taken into account or not, a second-order low-pass filter is implemented by the averaging of the noise. Besides, ripples are observed: frequencies that are multiple of $1/\tau$ are nullified. In addition, when calibration is considered, it creates in a second-order high-pass filter. The lowest frequencies are absorbed by the calibration. The lower the frequency, the better the compensation. Calibration-related ripples are also observed: for frequencies that are multiple of $1/T$, the current measure and the calibration one are in phase and cancel out.

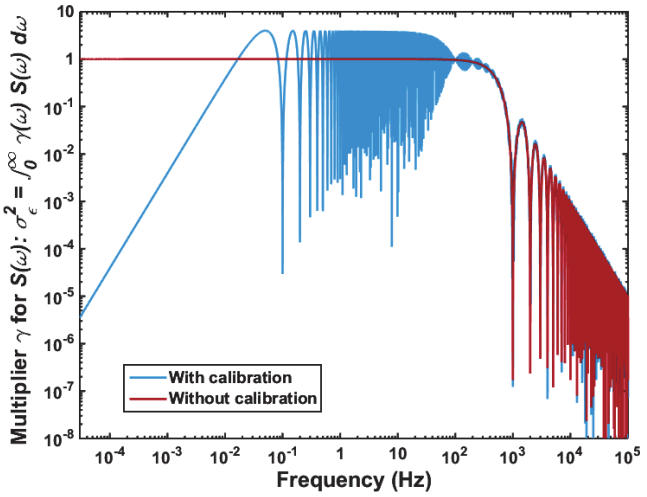

Fig. 1. Frequency-dependant weighting of the noise power spectral density, computed for $\tau = 1\,\mathrm{ms}$, $\tau_c = 10\,\mathrm{ms}$, $T_c = 10\,\mathrm{s}$.

One can also remark that the function G can be decomposed as:

$$G(u,x,y) = G_x(u,x) + G_y(u,x) - G_{x,y}(u,x,y)$$

with:

$$\begin{cases} G_x(u,x) = \frac{1}{(u\,x)^2}\Big(1-\cos(u\,x)\Big) \\ G_y(u,x) = \frac{1}{(u\,y)^2}\Big(1-\cos(u\,y)\Big) \\ G_{x,y}(u,x,y) = \frac{1}{u^2\,x\,y}\Big(\cos(u) + \cos(u\,(1+x-y)) - \cos(u\,(1+x)) - \cos(u\,(1-y))\Big) \end{cases}$$

On one hand, $G_x(u,x)$ and $G_y(u,x)$ describe the impact of noise during respectively the actual measurement and the calibration one, independently from one another. In fact, $\int_0^{\infty} 2\,S(\omega)\,G_x\left(\omega\,T_c, \frac{\tau}{T_c}\right)\mathrm{d}\omega$ gives the corresponding variance as expressed by (2). On the other hand, $G_{x,y}(u,x,y)$ corresponds to the impact of the correlation between those two measurements, and thus to how the calibration allows to reduce the variance in the obtained error.

III. Practical Formula

Using (5), the impact of pure white, pure flicker noise and low-pass filtered white noise can be computed. The obtained results are as follow.

• For white noise $S(\omega) = A$:

$$\sigma_\varepsilon^2 = A \cdot \pi \cdot \left(\frac{1}{\tau} + \frac{1}{\tau_c}\right) \tag{6}$$

This result matches what could be expected. During calibration and current measures, the noise leads to errors with variances $\frac{A\,\pi}{\tau_c}$ and $\frac{A\,\pi}{\tau}$ (as found in [8]). Since they are produced by white noise, these errors are uncorrelated, hence their variances add up.

• For flicker noise $S(\omega) = \frac{A}{\omega}$:

$$\sigma_\varepsilon^2 = A \cdot \zeta\left(\frac{\tau}{T_c}, \frac{\tau_c}{T_c}\right) \tag{7}$$

with:

$$\begin{aligned}\zeta(x,y) = \frac{1}{xy}\Big((1+x)^2 ln(1+x) \\ + (1-y)^2 ln(1-y) \\ - (1+x-y)^2 ln(1+x-y)\Big) \\ - ln(x\,y)\end{aligned} \tag{8}$$

Note that this formula cannot be used for $y = 1$ (i.e. when the actual measurement directly follows the calibration one). The suitable formula can be computed either from (5), either from (8) by computing $\lim_{y\to 1} \zeta(x,y)$. It leads to:

$$\zeta(x,1) = \frac{1}{x}\Big((1+x)^2 ln(1+x) - x^2 ln(x)\Big) - ln(x) \tag{9}$$

The obtained normalized variance σ_ε^2/A is depicted on Fig. 2.

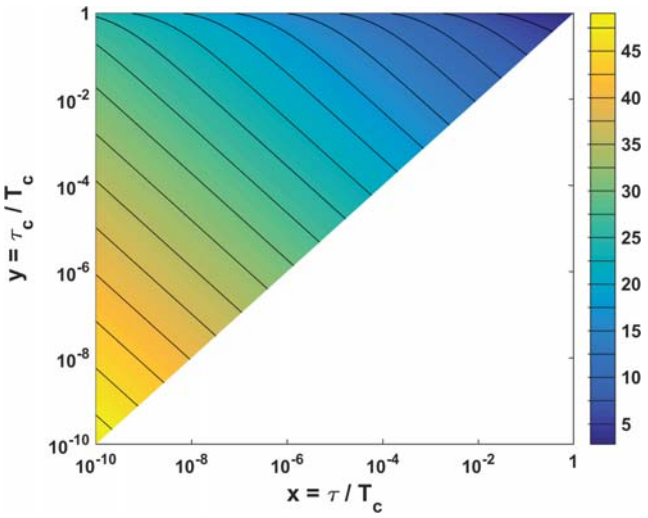

Fig. 2. Obtained normalized variance σ_ε^2/A with a noise of power spectral density $S(\omega) = \frac{A}{\omega}$

• For flicker noise $S(\omega) = \frac{A}{\omega^\alpha}$, with $\alpha \in\ ]0,2[\ \setminus\{1\}$:

$$\begin{aligned}\sigma_\varepsilon^2 = 2\,A \cdot \Gamma(-1-\alpha)\,\sin\left(\frac{\alpha\,\pi}{2}\right) \\ \cdot \Bigg[\tau_c^{\alpha-1} + \tau^{\alpha-1} \\ + \frac{T_c^{1+\alpha}}{\tau\,\tau_c}\xi\left(\frac{\tau}{T_c}, \frac{\tau_c}{T_c}, 1+\alpha\right)\Bigg]\end{aligned} \tag{10}$$

with:

$$\xi(x,y,a) = 1 + (1+x-y)^a - (1+x)^a - (1-y)^a \tag{11}$$

Typical obtained normalized variances $\sigma_\varepsilon^2/(A\,T_c^{\alpha-1})$ are depicted on Fig. 3 and Fig. 4, using respectively $\alpha = 0.9$ and $\alpha = 1.2$.

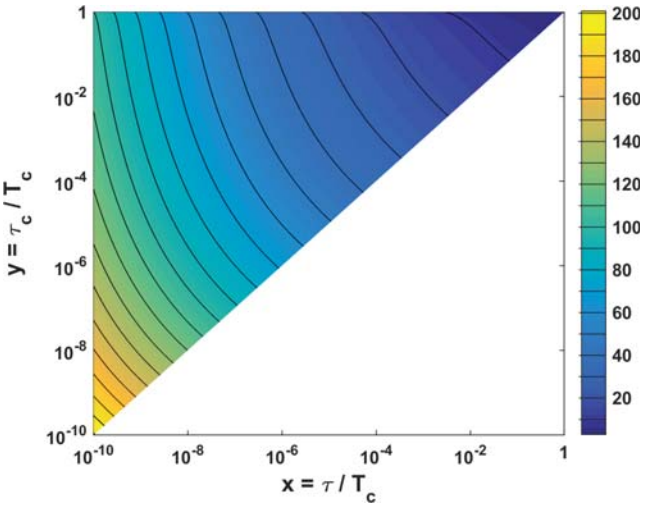

Fig. 3. Obtained normalized variance $\sigma_\varepsilon^2/(A\,T_c^{\alpha-1})$ with a noise of power spectral density $S(\omega) = \frac{A}{\omega^\alpha}$, with $\alpha = 0.9$

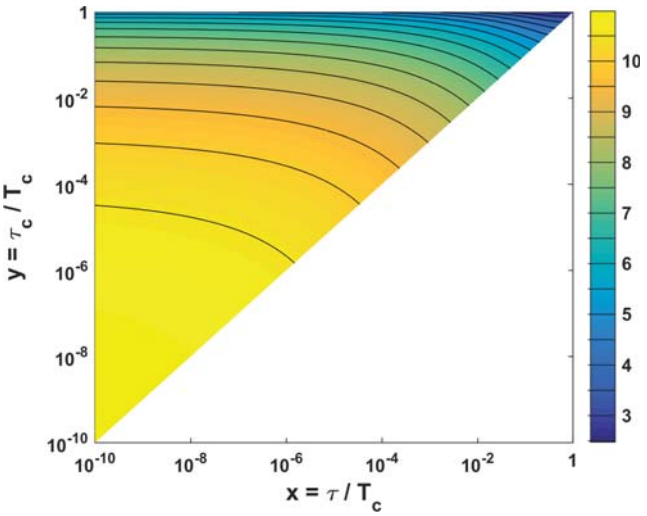

Fig. 4. Obtained normalized variance $\sigma_\varepsilon^2/(A\,T_c^{\alpha-1})$ with a noise of power spectral density $S(\omega) = \frac{A}{\omega^\alpha}$, with $\alpha = 1.2$

The figure Fig. 5 depicts how the flicker noise increases the variance of the error as the time since calibration passes, depending on its frequency exponent α.

• For white noise filtered by a first-order low-pass filter with a cutoff angular frequency ω_0 (as discussed in [7]), $S(\omega) = \frac{A}{1+\left(\frac{\omega}{\omega_0}\right)^2}$:

$$\sigma_\varepsilon^2 = A \cdot \pi\,\omega_0 \cdot \chi\big(\tau\,\omega_0, \tau_c\,\omega_0, (T_c - \tau_c)\,\omega_0\big) \tag{12}$$

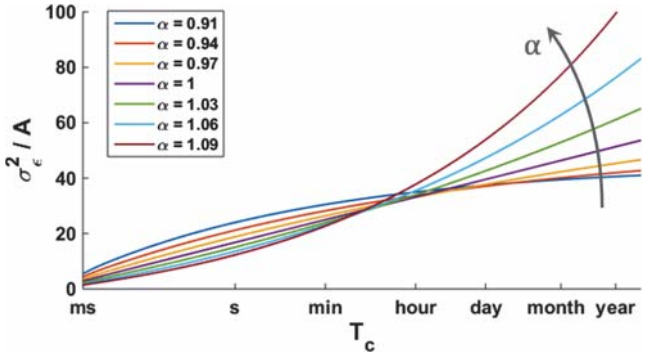

Fig. 5. Evolution of the variance σ_ε^2 due to different flicker noises $S(\omega) = \frac{A}{\omega^\alpha}$ as the time since calibration T_c increases, considering the case: $\tau = \tau_c = 1\,\text{ms}$

with:

$$\begin{aligned}\chi(a,b,c) = \quad & \frac{1}{a} + \frac{1}{a^2}\left(\mathbf{e}^{-a} - 1\right) \\ & + \frac{1}{b} + \frac{1}{b^2}\left(\mathbf{e}^{-b} - 1\right) \\ & - \mathbf{e}^{-c} \cdot \frac{1 - \mathbf{e}^{-a}}{a} \cdot \frac{1 - \mathbf{e}^{-b}}{b}\end{aligned} \tag{13}$$

We can note that, as expected, the two first lines in the expression of χ corresponds to the impact of the considered noise on the actual measurement and the calibration one respectively, independently from one another. In fact, applying (2) to the given power spectral density S leads to a variance for a single measurement:

$$\begin{aligned}\sigma_{\varepsilon,x}^2 &= A \cdot \frac{\pi}{\tau^2}\left(\tau + \frac{\mathbf{e}^{-\tau\,\omega_0} - 1}{\omega_0}\right) \\ &= A \cdot \pi\,\omega_0 \cdot \left(\frac{1}{a} + \frac{1}{a^2}\left(\mathbf{e}^{-a} - 1\right)\right)\end{aligned}$$

The third line in the expression of χ represents the reduction of the error thanks to calibration. It decreases exponentially as the time from the end of the calibration measurement to the beginning of the actual measurement increases. It also decreases as the integration times increases.

Besides, one can notice that when considering the limit case $\omega_0 \to \infty$ (hence $a, b, c \to \infty$), we find again what was obtained for the white noise (6). In fact, it gives: $\chi(a,b,c) \overset{\omega_0 \to \infty}{\sim} \frac{1}{a} + \frac{1}{b}$; and so: $\sigma_\varepsilon^2 \overset{\omega_0 \to \infty}{\sim} A \cdot \pi \cdot \left(\frac{1}{\tau} + \frac{1}{\tau_c}\right)$.

IV. Implementation

Since $0 < \tau \leq \tau_c \leq T_c$, $\zeta(x,y)$ and $\xi(x,y,a)$ shall be computed for $0 < x \leq y \leq 1$ and $a \in\ ]1,3[\ \setminus\{2\}$. Some precautions should be taken. In fact, depending on the application, one may consider for the elapsed time T_c since calibration to reach months or even years. This may be the case for example for biomedical implanted chips. In such conditions, $x = \tau/T_c$ and $y = \tau_c/T_c$ become extremely small. Then, in (8), (9) and (11), subtracted terms cancel out to give results that are far bellow the initial values.

However, the computing software has a finite resolution, limited by the number of bits b of the significand. With double precision (i.e. 64-bits floats), which is the case in MATLAB: $b = 52$. As a result, a value v is stored with a maximal error $\epsilon_{max}(v) = 2^{-\lfloor b+2-log_2(v)\rfloor} \leq \frac{v}{2^{b+1}}$. So computing $v - w$ can lead to a relative error up to $\frac{v}{v-w}\frac{1}{2^{b+1}}$ that might be too large if $v \approx w$.

Thus, for low values of x and potentially y, using the original, ideal formulas (8), (9) and (11) may lead to erroneous results. In such cases, it is required to use an alternative implementation. To do so, these formulas are approximated using Taylor series. Then to ensure reliable implementations for $\zeta(x,y)$ and $\xi(x,y,a)$, the error associated with each possible formula is estimated. Depending on the case, it is the error due to the approximation, the error due to the finite resolution for the manipulated numbers, or a sum of both. The formula providing the least error is used.

A. Implementation of $\zeta(x,1)$

The original formula for $x \mapsto \zeta(x,1)$ was:

$$\zeta(x,1) = \frac{1}{x}\Big((1+x)^2 ln(1+x) - x^2 ln(x)\Big) - ln(x) \tag{9}$$

Due to the aforementioned resolution issue, this formula is associated with a bit-related error:

$$\varepsilon_{(9)} \leq \frac{1}{2^{b+1}x}$$

However, when $x \ll 1$:

$$\zeta(x,1) = 1 - ln(x) + (3/2 - ln(x))\,x + O(x^2)$$

Thus, one can use the approximation:

$$\zeta(x,1) \approx 1 - ln(x) \tag{14}$$

with an error:

$$\varepsilon_{(14)} \approx \left(\frac{3}{2} - ln(x)\right) x$$

So the implementation for $\zeta(x,1)$ shall use (14) when $\left(\frac{3}{2} - ln(x)\right) x < \frac{1}{2^{b+1}x}$, and (9) else.

The next sections use the same reasoning that will not be detailed again. Only the formulas (i) and the associated errors $\varepsilon_{(i)}$ will be provided. For each situation, the formula (i) to use is the one providing the minimal $\varepsilon_{(i)}$.

B. Implementation of $\zeta(x,y)$, $y < 1$

The original formula for $(x,y) \mapsto \zeta(x,y)$ was:

$$\begin{aligned}\zeta(x,y) = \frac{1}{xy}\Big(&(1+x)^2 ln(1+x) \\ &+ (1-y)^2 ln(1-y) \\ &- (1+x-y)^2 ln(1+x-y)\Big) \\ &- ln(x\,y)\end{aligned} \tag{8}$$

This formula is associated with a bit-related error:

$$\varepsilon_{(8)} \leq \begin{cases} \frac{1}{2^{b+1}\,x\,y}\,, & \text{if: } y - x < 2^{-b-2} \\ \frac{1}{2^{b+1}\,x\,y}(1 - (1-y)(1-y+(6-4y)\ln(1-y)))\,, & \\ & \text{else}\end{cases}$$

For $x \ll 1$, (8) becomes:

$$\zeta(x,y) \approx 1 + \frac{2y - x - 2}{y}\, ln(1-y) - ln(x\,y) \tag{15}$$

with a maximal error:

$$\varepsilon_{(15)} \approx \frac{x^2}{3\,(1-y)} + \frac{1}{2^{b+1}\,y}$$

For $x \leq y \ll 1$:

$$\zeta(x,y) \approx 3 + x - y - ln(x\,y) \tag{16}$$

with an error:

$$\varepsilon_{(16)} \approx \frac{(y-x)^2 + x\,y\,/\,2}{3}$$

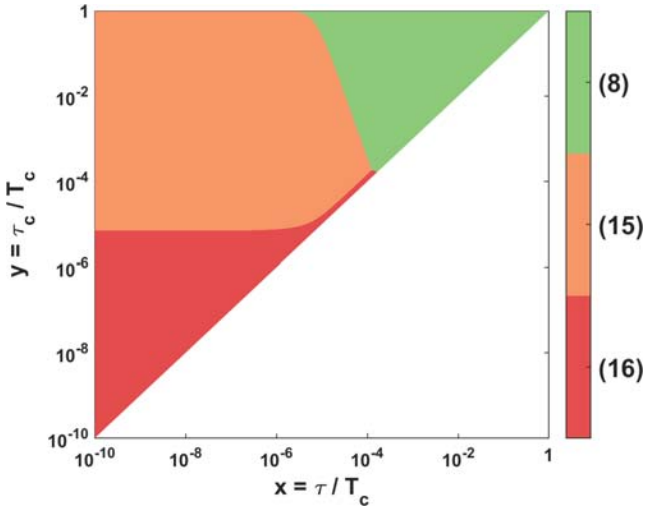

Fig. 6. Used formula for computing $\zeta(x,y)$, depending on x and y

C. Implementation of $\xi(x,y,a)$, $y < 1$

The original formula for $(x,y,a) \mapsto \xi(x,y,a)$ was:

$$\xi(x,y,a) = 1 + (1+x-y)^a - (1+x)^a - (1-y)^a \tag{11}$$

Due to the finite resolution of the computing software, it is associated with an error:

$$\varepsilon_{(11)} \leq \begin{cases} \frac{4}{2^b} & \text{if } 1 < a < 2 \\ \frac{1}{2^b} & \text{else} \end{cases}$$

When $x \ll 1$:

$$\xi(x,y,a) \approx -ax + (1+x-y)^a - (1-y)^a \tag{17}$$

with a maximal error:

$$\varepsilon_{(17)} \approx a\,(a-1)\,\frac{x^2}{2} + \frac{1}{2^{b+1}}(a+2)(1-y)^{a-1}$$

When also $x \ll 1-y < 1$:

$$\xi(x,y,a) \approx \left((1-y)^{a-1} - 1\right) a\; x \tag{18}$$

with a maximal error:

$$\varepsilon_{(18)} \approx a\,(a-1)\,\left|(1-y)^{a-2} - 1\right|\,\frac{x^2}{2} + \frac{a}{2^{b+2}}$$

Also, for $x \leq y \ll 1$:

$$\xi(x,y,a) \approx -a\,(a-1)\,x\,y \tag{19}$$

with an error:

$$\varepsilon_{(19)} \approx a\,(a-1)\;|a-2|\;\frac{xy}{2}\left(y - x + \left(1 - \frac{a}{3}\right)\frac{xy}{2}\right)$$

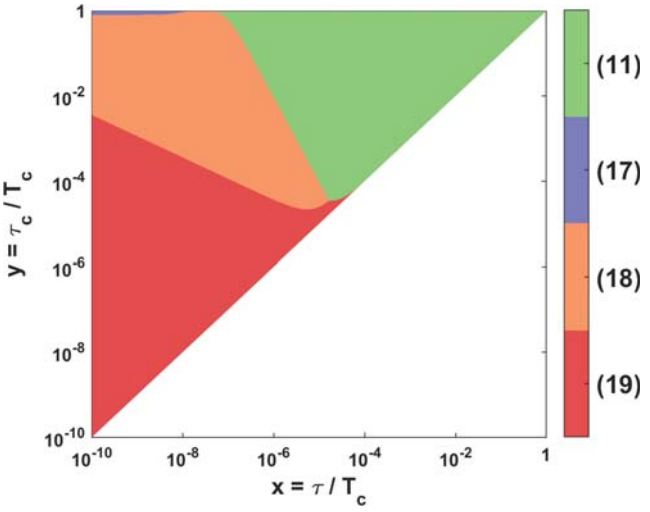

Fig. 7. Used formula for computing $\xi(x,y,a)$ with $\alpha = 0.9$ (hence $a = 1.9$), depending on x and y

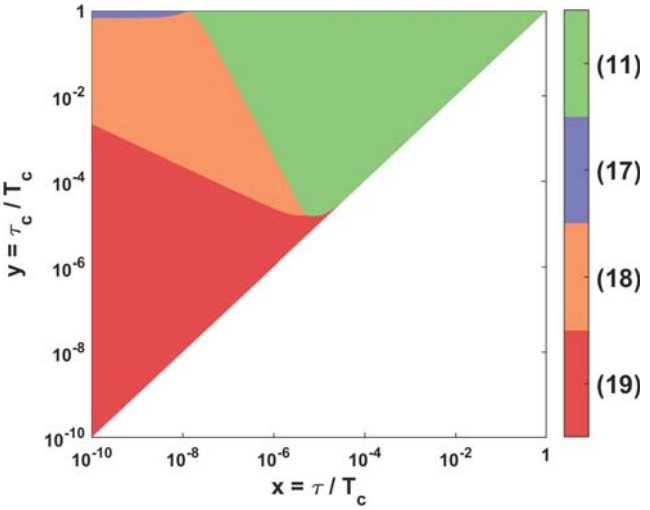

Fig. 8. Used formula for computing $\xi(x,y,a)$ with $\alpha = 1.2$ (hence $a = 2.2$), depending on x and y

D. Implementation of $\chi(a,b,c)$

The original formula for $(x,y,a) \mapsto \zeta(x,y)$ was:

$$\begin{aligned} \chi(a,b,c) = \quad & \frac{1}{a} + \frac{1}{a^2}\left(\mathbf{e}^{-a} - 1\right) \\ & + \frac{1}{b} + \frac{1}{b^2}\left(\mathbf{e}^{-b} - 1\right) \\ & - \mathbf{e}^{-c} \cdot \frac{1 - \mathbf{e}^{-a}}{a} \cdot \frac{1 - \mathbf{e}^{-b}}{b} \end{aligned} \tag{13}$$

Though in previous sections, $x \ll 1$ and $y \ll 1$ corresponded to typical cases that can be encountered in practice, the cases $a \ll 1$ and $b \ll 1$ are less likely to occur. However, for the sake of being as exhaustive as possible, we will discuss the considerations concerning the implementation of χ in order to handle such situations.

Concerning the first and second lines in the formula (13), it has to be noticed that the formula:

$$\left(\frac{1}{a}+\frac{1}{a^2}\left(\mathbf{e}^{-a}-1\right)\right) \tag{20}$$

or equivalently:

$$\frac{\mathbf{e}^{-a}-1+a}{a^2} \tag{20'}$$

is associated when $a \ll 1$ to a bit-related error:

$$\varepsilon_{(20)} \leq \frac{1}{2^{b+2}\,a^2}$$

Nevertheless, it can be approximated as:

$$\left(\frac{1}{a}+\frac{1}{a^2}\left(\mathbf{e}^{-a}-1\right)\right) \approx \frac{1}{2} \tag{21}$$

with an approximating error:

$$\varepsilon_{(21)} \approx \frac{a}{6}$$

Thus, approximation (21) will be preferred for computing the term (20) when: $a \leq \left(\frac{3}{2^{b+1}}\right)^{1/3} \approx 6.932 \cdot 10^{-6}$ (with $b = 52$).

Concerning the third line of in the formula (13), we remark that:

$$\frac{1-\mathbf{e}^{-a}}{a} \tag{22}$$

is associated to an error:

$$\varepsilon_{(22)} \leq \frac{1}{2^{b+2}\,a}$$

while it can be approximated as:

$$\frac{1-\mathbf{e}^{-a}}{a} \approx 1 \tag{23}$$

with an error:

$$\varepsilon_{(21)} \approx \frac{a}{2}$$

Thus, approximation (23) will be preferred for computing the term (22) when: $a \leq 2^{-\frac{b+1}{2}} \approx 1.054 \cdot 10^{-8}$ (with $b = 52$).

Note that no specific issue arise from $c \ll 1$ or $c \gg 1$.

V. Conclusion

In continuous-time integrator-based ADCs, the input-referred noise is integrated along with the input signal, resulting in a random Gaussian error. For a proper estimation of its standard deviation, the calibration process of the converter must be taken into account. The results are in fact highly dependent on both the integration time and the elapsed time since calibration. Here, it has been assumed that the calibration consists in a simple measure whose result is subtracted to the current measure. The corresponding theory has been developed and led to formulas for computing the effect of white noise, flicker noise and low-pass filtered white noise on the accuracy of the converter. Using them requires some programming precautions, but the latter have been addressed.

Acknowledgment

The authors acknowledge the financial support of the Swiss National Science Foundation (SNSF) under founding no. CR23I3_157023.

References

[1] Paul Jespers. *Integrated converters: D to A and A to D architectures, analysis and simulation*. Vol. 11. Oxford University Press, 2001. ISBN: 978-0198564461.

[2] Gabriele Manganaro. *Advanced data converters*. Cambridge University Press, 2012. ISBN: 978-1107005570.

[3] Syed K. Islam et al. "Integrated circuit biosensors using living whole-cell bioreporters". IEEE Transactions on Circuits and Systems I: Regular Papers, Vol. 54, No. 1, Jan. 2007, pp. 89-98.

[4] Yevgeny Perelman and Ran Ginosar. "A low-light-level Sensor for medical diagnostic applications". IEEE Journal of Solid-State Circuits, Vol. 36, No. 10, Oct. 2001, pp. 1553-1558. doi: 10.1109/4.953484.

[5] Ritu Raj Singh et al. "A CMOS $\Sigma - \Delta$ photodetector array for bioluminescence-based DNA sequencing". Symposium on VLSI Circuits-Digest of Technical Papers, June 2011, pp. 96-97.

[6] Horst Zimmermann. *Silicon Optoelectronic Integrated Circuits*. Springer Science & Business Media, 2004. ISBN: 3-540-40518-6.

[7] Philip R. Westlake. "The Effects of Noise through an Analog Integrator Which Integrates with Respect to an Arbitrary Variable". IRE Transactions on Aerospace and Navigational Electronics, Vol. ANE-9, No. 3, Sept. 1962, pp. 151-158.

[8] Emily J. McDowell et al. "A generalized noise variance analysis model and its application to the characterization of 1/f noise". Optic Express, Vol. 15, No. 7, Apr. 2007, pp. 3833-3848.

Paul Gosselin graduated as engineer at École Polytechnique (Palaiseau, France) and received the M.S. degree in Electrical Engineering from École Polytechnique Fédérale de Lausanne (EPFL, Switzerland). He is currently working towards the PhD degree, still at École Polytechnique Fédérale de Lausanne, making use of his background in mathematics and in computer science in order to achieve proper modeling of the considered systems and to develop tools and strategies for helping the search for optimal designs.

Maher Kayal received M.S. and Ph.D degrees in electrical engineering from the École Polytechnique Fédérale de Lausanne (EPFL, Switzerland) in 1983 and 1989 respectively. He has been with the Electronics laboratories of the École Polytechnique Fédérale de Lausanne (EPFL, Switzerland) since 1990, where he is currently a professor and director of the "Energy Management and Sustainability" section. He has published many scientific papers, coauthor of three text books dedicated to mixed-mode CMOS design and he holds 10 patents. His technical contributions have been in the area of analog and mixed-signal circuits design including highly linear and tunable sensors microsystems, signal processing and green energy management.

Adil Koukab received the MSc and Ph.D. degree in electrical engineering from the University of Nancy-Metz and Supélec, France in 1993 and 1998. He is currently a Research Associate and project leader at the Department of Electrical Engineering of the Swiss Federal Institute of Technology in Lausanne (EPFL). His research interests include: Devices and circuits for Optics and photonics, RF and analog design for wireless communications (GSM, UMTS, WLAN, Bluetooth, UWB…); Noise in Mixed-Signal and RF System-on-chip; Devices Physics and modeling, Numerical and computational methods: Spectral Method, Boundary Element Method. He has several publications in these domains. He also participates regularly to the technical program committees of a number of conferences and workshops and served as reviewer for IEEE journals including JSSC, MTT and MWCL.